ACS APPLIED OPTICAL MATERIALS

pubs.acs.org/acsaom Article

Unveiling Coupled Anapole Modes in Ultrananocrystalline Diamond

Edgar Palacios, Anirudha V. Sumant, Akshay A. Murthy, Sina Abedini Dereshgi, Vinayak P. Dravid, and Koray Aydin*

Cite This: *ACS Appl. Opt. Mater.* 2023, 1, 1627−1633 Read Online

ACCESS | Metrics & More | Article Recommendations | Supporting Information

ABSTRACT: Recently, optical phenomena generated by interfering electric and magnetic modes through the use of high-index dielectric materials have garnered significant attention. Destructive interference of scattered fields produced using toroidal loops of electric or magnetic fields known as anapole modes is one such nontrivial effect. Here, we demonstrate the viability of ultrananocrystalline diamond for metasurface applications and the potential it offers for coupling anapole modes. Because such modes are confined within the disks, coupling between this mode and the absorption and emission modes of MoS_2 induces an enhancement in the photoluminescence. This high-density, subwavelength light−matter interaction method serves as a platform toward mitigating the lossy effects inherent to traditional plasmonic materials while spatially confining the mode plasmonic modes in an effort to achieve more efficient methods of enhancing light−matter interactions.

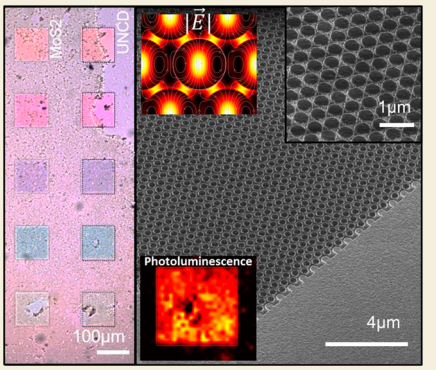

KEYWORDS: *anapole mode, ultrananocrystalline diamond, high-index dielectrics, metasurface, MoS_2*

INTRODUCTION

To date, research on plasmonics has enabled a plethora of photonic applications thanks to the near-field confinement and increased local photonic density of states generated. These applications include lasers,[1−3] photodetectors,[4−6] energy harvesting,[7−9] biosensors,[10] and chemical sensors among others. The most commonly used metals, Au and Ag, however, suffer from two key disadvantages inherent to plasmonic metals: Joule losses and low melting temperatures. These losses in metals impede their application for technologies with light below the diffraction limit, since almost half of the total energy is stored in the form of kinetic energy and is therefore subjected to loss mechanisms, such as phonon-assisted absorption, electron−electron scattering, Landau dampening, and interband absorption.[11] This can lead to localized heating[12−14] that can be undesirable in temperature sensitive samples and can cause deformation of nanostructures and reduced optical performance over time. Further, the inherent low melting temperature of bulk noble plasmonic metals makes these systems incompatible for high operational temperature and/or power applications, such as heat-assisted magnetic recording[15] and thermophotovoltaics.[16] This aspect is further exacerbated by the fact that melting temperature scales inversely with particle size.[11] Because of these aspects, plasmonic materials such as titanium nitride, which exhibits a bulk melting temperature of 2073 °C (~90% higher than Au) have emerged as promising alternatives. Titanium nitride has been shown to achieve similar plasmonic performance to Au but has the added benefit that it can retain optical performance and structure.[17] Such alternatives improve the current state of plasmonics with respect to practicality but still fail to address the inherent losses in metals.

In the quest to solve both drawbacks of plasmonics, high-index dielectric materials represent a favorable option. These materials exhibit low losses and have been employed widely in large scale processing due to their higher melting temperatures compared to traditional plasmonic materials.[18,19] Although Si and TiO_2 represent excellent alternatives for applications such as perfect reflectors[20−22] and enhanced light−matter interactions,[23−25] the bulk of current studies associated with these systems have demonstrated strong dipolar and multipolar electric and magnetic resonances that manifest when the thickness of the material generally exceeds several hundred nanometers. This leaves high density and sub-100 nm resolution metasurfaces to be explored where electric and magnetic fields can interfere spatially and spectrally. In such a scenario, one can obtain temperature-insensitive and low-loss optical devices that are compatible with continued device miniaturization demands.

One such optical mode that is dominant in thin nanostructured dielectric materials is the anapole mode. This mode is composed of electric and toroidal dipole moments whose radiation patterns destructively interfere when the moments

Received: February 22, 2023
Revised: September 15, 2023
Accepted: September 27, 2023
Published: October 16, 2023

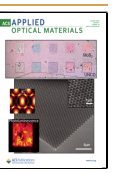

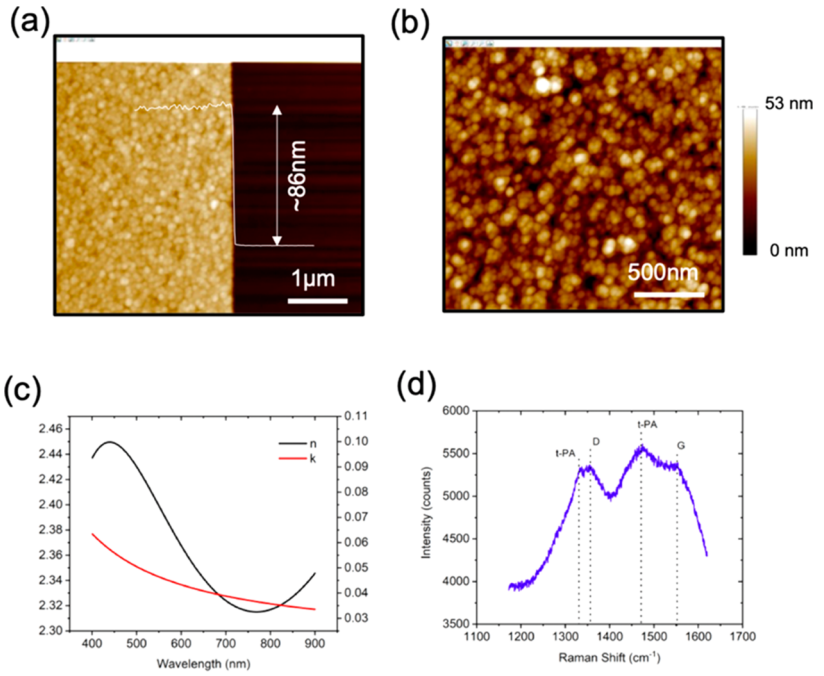

Figure 1. Characterization of the thin film-UNCD. (a) AFM image of UNCD thickness showing a line profile of UCND height. (b) 2 × 2 μm^2 AFM image used to calculate surface roughness of 15.25 nm rms and mean UNCD cluster size of 64 nm. (c) Calculated refractive index data using spectroscopic ellipsometry. (d) Raman spectra of the same UNCD.

are out of phase and are spectrally overlapped, with the signature of minima of radiation in the far-field.[26] Experimental demonstrations of anapole modes have been shown using single nanodisks of Si[27,28] or Ge.[29] In addition, such modes also largely confine electric fields within the structure, contrary to resonant plasmonic modes where field enhancements are confined to the surfaces. Because of this, such modes have been shown to be useful in applications where electric field enhancement is required such as lasing,[28] efficient third harmonic generation,[29] biosensing,[30] molecular excitonic resonance coupling,[31] as well as memory applications thanks to the combined electric and magnetic response of anapole modes.[32] Recent advances demonstrating the potential of coupling the emissive modes in layered van der Waals, in particular, exciton modes in metal dichalcogenides, with plasmonic and Mie modes[33] as well as other well-established modes such as cavity[34] and grating[35] modes provide unique potential for the compact on-chip photonics of the next generation.[33]

In this work, we aim to explore the optical behavior of high-index metasurfaces composed of close-packed ultrananocrystalline diamond nanodisks. By designing high-index materials with subwavelength thicknesses and reducing the distance between disks, we uncover coupling between optical anapole modes. Various arrays of these nanodisks with diameters varying from 350 to 450 nm are fabricated and demonstrate anapole modes between 500 and 700 nm that manifest as transmission minima. Moreover, because of the confined nature of electric and magnetic fields within the nanodisks, these modes are shown to be sustained with a small spectral shift despite surface and sidewall roughness. Finally, as a proof of concept, we combine these arrays with single layer MoS_2 to demonstrate that coupling through anapole modes leads to an enhancement in the photoluminescence signal due to increases in the absorption or emission rates.

RESULTS AND DISCUSSION

The base of our samples begins with 86 nm thick ultra nanocrystalline diamond (UNCD) grown on fused quartz via microwave plasma chemical vapor deposition (MPCVD). To characterize the surface roughness of UNCD, atomic force microscopy measurements were taken from a 2 × 2 μm^2 area near the fabricated arrays shown in Figure 1a,b. These measurements showed a surface root mean squared roughness of ∼15.25 nm, 86 nm thickness, and mean UNCD cluster size of 64 nm, which is consistent with previous reports of UNCD grown using MPCVD.[36] Optical properties of UNCD were also measured using spectroscopic ellipsometry, which gives us the spectral dependence of the material between 400 and 900 nm (Figure 1c). The obtained spectra were then fitted to the empirical Cauchy absorbent model to achieve a mean squared error below 10% and were best when compared to Gauss and harmonic oscillator models. The measured refractive index within the 400−900 nm spectral range is between 2.31 and 2.45, and the optical extinction is between 0.03 and 0.06. It is worth noting that the obtained n,k model for UNCD is slightly different from previous reports[36] This discrepancy is attributed to the roughness and grain sizes, which is common for materials with deposition-dependent noncrystallinity.[37] Raman scattering spectra were also taken from the same area as shown in Figure 1d. These measurements were taken using a 545 nm laser over a spectral range between 1172 and 1620 cm^{-1}. The measured Raman spectra exhibit several prominent peaks characteristic of diamond, nanodiamond, and *trans*-polyscetylene. In addition, D and G band peaks near 1356 and 1552 cm^{-1} are also visible, which correspond to the existence of intergranular phases that arise from sp^2 and stretching and breathing modes, respectively.[36]

Hexagonally packed nanodisks are fabricated in UNCD with diameters ranging from 350−450 nm in 50 nm increments. SEM images show roughness at the disk perimeter, which is a

https://doi.org/10.1021/acsaom.3c00071
ACS Appl. Opt. Mater. 2023, 1, 1627−1633

consequence of the polycrystalline nature of UNCD (Figures 2a,b). This roughness thus varies the gap distance between 35

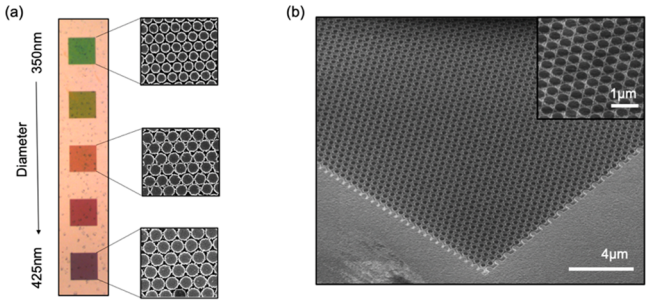

Figure 2. (a) Optical image in reflection mode of postfabricated UNCD arrays ranging from 350−450 nm in diameter. (b) Perspective SEM micrograph of UNCD array. Inset shows magnified view of each array.

and 100 nm with a median value of ∼65 nm. Postfabrication, optical inspection of the sample in reflection mode shows a range of colors varying from green to deep red that indicate optical modes spanning the visible range (Figure 2a).

In order to understand the optical phenomena occurring in close-packed arrays, we start by analyzing the optical modes present in single disks. FDTD simulations are conducted on smooth single disks using an experimentally obtained UNCD refractive index, and scattering spectra are calculated for each independently. Calculated scattering spectra shown in Figure 3a exhibit local minima in scattering that redshift from 545 to 650 nm as the diameter of the disk is increased. In the case of resonant modes in plasmonic nanoparticles, peaks in the scattering spectra result from enhanced scattering in the plasmonic mode. Here, however, in the case of dielectric metasurfaces, minima in scattering are a representation of a nontrivial interaction between electric and magnetic loops that generate destructively interfering far-field radiation patterns as has been shown experimentally in single nanodisks.[38,39] In this specific case, the electric fields form toroidal electric field loops and create electric and magnetic dipole moments, as seen in Figure 3b,c.

To see how these modes interact with each other, a series of arrays were prepared with 350 nm diameter disks with a gap distance that was varied between 50 and 350 nm (Figure 3d). The arrays were illuminated with a plane wave source coming from the nanostructured UNCD side, and transmission was calculated through the UNCD and glass substrate. At a gap distance of 350 nm, transmission throughout the entire visible spectrum is over 75%, with a weak transmission minimum close to 840 nm. This weak minimum indicates that for gap distances on this length scale, coupling of far-field light to the nanostructured UNCD as well as interparticle coupling is minimal. However, as gap distance is decreased, the initially weak transmission minimum blueshifts linearly and decreases before ultimately approaching a minimum transmission of near zero. More interestingly, below a gap distance of ∼125 nm, a secondary minimum appears that exhibits dispersive-like behavior and blueshifts as the gap distance continues to decrease. By looking at the magnetic and electric field profiles (Figure 3e,f) through the UNCD disks at a gap distance of 50 nm where the two modes are separated enough spectrally, we can see an existence of two similar field profiles that occur due to different distributions of electric and magnetic field loops. At 505 nm, the calculated magnetic field profiles (Figure 3e) show the existence of toroidal loops, indicating that as gap distances are reduced, coupling between disks begins to yield magnetic anapoles. This hybrid mode is distinct from the electric anapole mode such that the electric field enhancement lies in the gaps rather than in the disk much like plasmonics

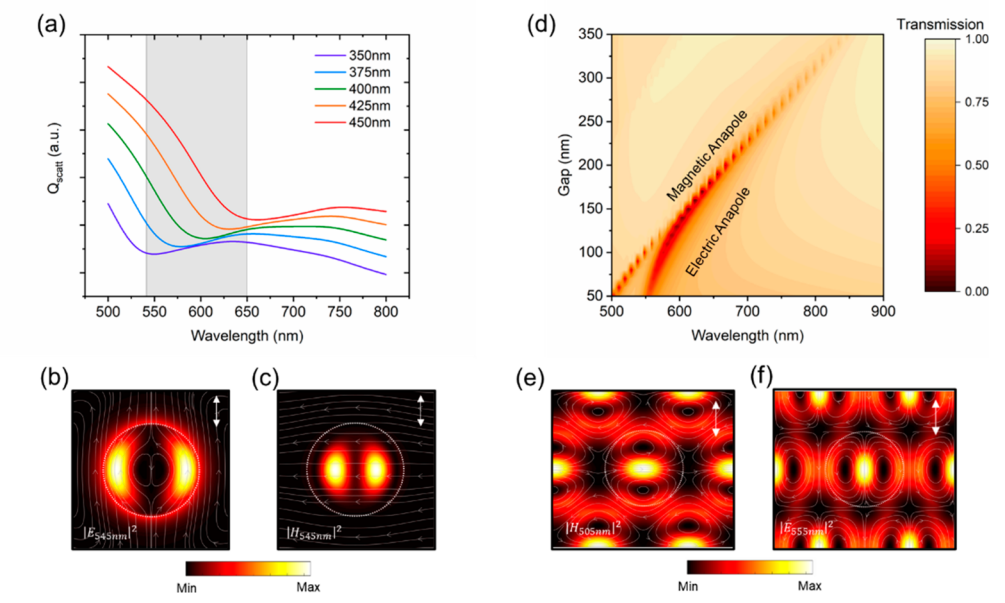

Figure 3. Theoretical calculations of single disks and arrays. (a) Single disk scattering spectra for single disks ranging from 350−450 nm in diameter. In-plane (b) electric and (c) magnetic field intensity plots with field lines taken through single UNCD disks. (d) Transmission map of 350 nm diameter arrays with gap varying between 50 and 350 nm. In-plane (e) magnetic and (f) electric field intensity plots with field lines taken through a unit cell of 350 nm diameter UNCD disk arrays with 50 nm gap. The dashed white circles in field intensity plots (b,c) and (e,f) represent the nanodisk boundaries. The arrow insets in field intensity plots (b,c) and (e,f) represent the polarization of the incident linear electric field impinging on the surface from the out-of-plane direction.

https://doi.org/10.1021/acsaom.3c00071
ACS Appl. Opt. Mater. 2023, 1, 1627−1633

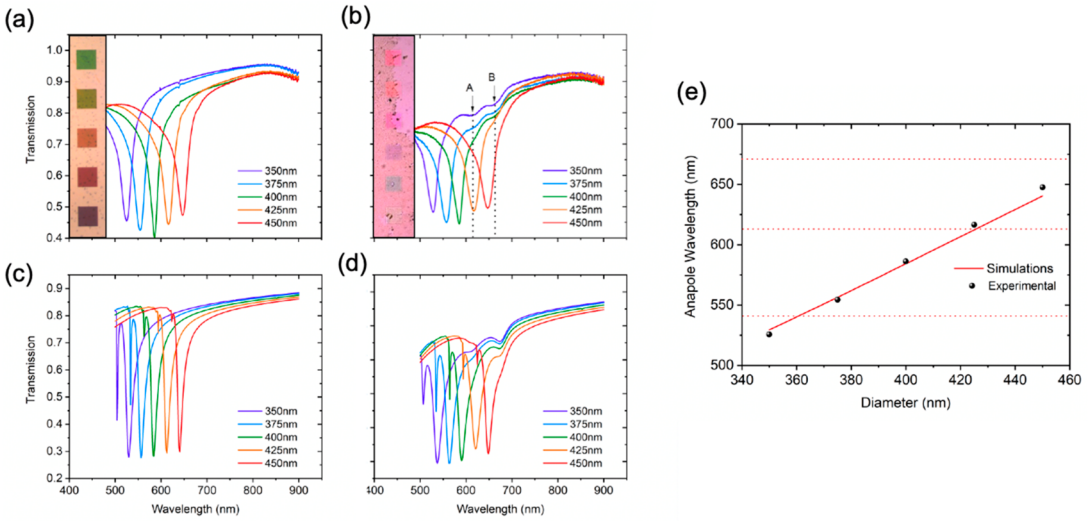

Figure 4. Experimental transmission measurements of (a) bare UNCD arrays and (b) MoS_2 covered arrays. Insets show optical images of samples before and after MoS_2 transfer. Theoretically calculated (a) bare UNCD arrays and (b) MoS_2 covered arrays. (e) Experimental and theoretical electric anapole mode wavelengths for arrays. Horizontal dotted lines in (e) represent excitation as well as A and B exciton wavelengths.

arrays.[38] Thus, the linear behavior of this mode is attributed to the gap distance as with plasmonic lattice modes. Contrary to that, the transmission minima at 555 nm exhibit a toroidal loop in the electric field profile (Figure 3f). Thus, this is believed to be the result from the electric anapole mode seen in the single disk case.[39] As the nanodisk gap distance is reduced, the disks begin to couple magnetically, giving rise to the dispersive-like shift in mode energy. This magnetic coupling is more evident when gaps between nanodisks are modified in the direction of magnetic field polarization as seen in Supporting Information, Figure S1.

To confirm the theoretical predictions, optical characterization of the fabricated arrays was conducted by measuring the transmission through the UNCD structure. A broadband halogen light source is incident from the nanostructured side and is linearly polarized, identical to the simulated structures. As the diameter is varied from 350 to 450 nm, a single transmission minimum corresponding to the electric anapole mode is observed and shifts from 525 to 647 nm (Figure 4a). Theoretical simulations of rough arrays yield similar results and correlate well with experimental observations of minima position (Figure 4e) and shape as shown in Figure 4b (see Figures S3−5). However, deviations between experimental and theoretical simulations were observed in relation to the magnetic anapole modes. The magnetic anapole mode is strongly suppressed in rough UNCD due to the fact that unlike the electric anapole mode where the electrical toroidal field is confined in the particle, the magnetic toroidal field can be outside the nanoantennas.[39] In simulations of rough UNCD, magnetic anapole modes were weaker than in the smooth case but were not observable in experimental measurements. This shows that while theoretical simulations show a trending behavior toward the unobservability of the magnetic anapole, the effect is more pronounced in experiment. It is posited to be due to the truly random nature of surface roughness in real samples, whereas theoretical simulation can be semirandom at best, since only a single unit cell is simulated and is set to be periodic (Supporting Information, Figures S3−5).

Although the electric anapole modes were shown to contain the electric field distribution mostly within the disk, a thin dispersive material like single layer MoS_2 could potentially still benefit from this confinement. Thus, as a proof of concept, single layer MoS_2 synthesized by chemical vapor deposition[40] was transferred on top of all nanodisk arrays using a polycarbonate-based transfer technique[41] and optically characterized starting with transmission measurements (Figure 4b). After transfer, transmission measurements for all arrays showed transmission profiles and minima positions almost identical to those prior to adding MoS_2 (Figure 4a). This is contrary to how a MoS_2/plasmonic array structure would react because the electric fields lie at the surface of the plasmonic material making the resonances extremely sensitive to changes in refractive index and surface roughness.[42] In this case, we do not observe such an effect but instead only observe a slight overall decrease in transmission due to intrinsic absorption of MoS_2 and the distinct A and B excitonic absorption peaks near 615 and 670 nm as seen in Figure 4b.

Photoluminescence (PL) measurements were taken for all arrays using a linearly polarized 545 nm laser source. Figure 5a shows the image of the measured PL map areas of the MoS_2 emission occurring on and off the UNCD arrays. To show the enhancement provided by the UNCD nanostructures, each map is presented as the PL enhancement, which is the ratio of PL on the array and on unstructured UNCD within each map, i.e., inside the white dashed squares in Figure 5b. Choosing to normalize the PL by a nearby area (right outside the white dashed squares in Figure 5b) is important, as it is well-known that the emission intensity of MoS_2 films grown through chemical vapor deposition can vary with position.[43] The maximum PL enhancement seen in all samples is 11, which occurs for the 450 nm diameter array (Figure 5b). This, however, is isolated as with many of the peak PL enhancements among all maps. To mitigate this, PL enhancement was evaluated by analyzing the histogram of pixel intensities within each map to get the minimum, maximum, and mean PL enhancement of each. From these results, it becomes clear as seen in Figure 5d that two PL maxima occur as we vary the disk diameter. To explain these results, we examined the theoretical electric field enhancements within MoS_2 at various key energies as a function of the disk diameter. The energies

https://doi.org/10.1021/acsaom.3c00071
ACS Appl. Opt. Mater. 2023, 1, 1627−1633

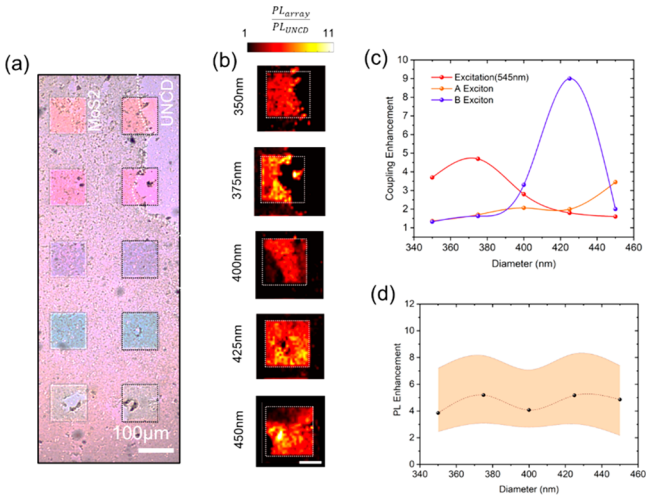

Figure 5. (a) Optical image of MoS_2 covered UNCD arrays. (b) 150 × 150 μm PL enhancement maps for 350−450 nm diameter UNCD arrays excited using 545 nm laser source with 0.75 NA objective. (c) Theoretical electric field enhancements in MoS_2 at excitation, A exciton, and B exciton wavelengths for each array. (d) PL enhancement containing mean, min, and maximum values for each array. The white dashed squares in (b) mark the patterned areas, which lead to PL enhancement.

included were at the laser wavelength as well as the A and B excitons, which are plotted in Figure 5c. The results here show that at lower diameter nanodisks, excitation enhancement is dominant peaking for the 375 nm disk array. This is caused by the spectral overlap of the confined electric anapole mode (Figure 3f) with the excitation source as seen in Figure 4b, which enhances the excitation rate in MoS_2. The second maximum then occurs at 425 nm. Contrary to the smaller arrays, simulations predict that excitonic coupling with the anapole mode is the dominant factor. Although theoretical results presented here drastically overestimate the enhancement because the simulations use a plane wave source instead of a dipole source where extraction efficiency and Purcell factor are more accurate predictors of emission rate enhancement, it is clear that excitonic coupling is the key driver of PL enhancement for the 425 and 450 nm arrays.

CONCLUSION

In summary, the transmission minima observed for all arrays originate from the coupling of electric anapole modes in close-packed UNCD nanodisks. This coupling is an interaction between magnetic and electric field loops that exhibit near-field confinement of light within the nanodisks. This is demonstrated by combining arrays with single layer MoS_2, which generate peak mean PL enhancements of ∼5 by tuning the anapole mode to selectively enhance absorption or emission rates. Although this work was based on UNCD structures, the underlying mechanisms are expected to occur in other commonly used materials such as TiO_2 and Si after careful consideration of the dimensions due to refractive index differences. The confinement effects exhibited here can lead to future applications of strong light−matter interactions including lasing, sensing, nonlinear optical phenomena, and high-powered optics.

METHODS

Fabrication

UNCD was deposited on a quartz substrate in a Lambda Microwave Plasma CVD system. The microwave plasma power was set to 2100 W, and the substrate was kept at the temperature of 800 °C. The chamber pressure was 120 mbar, and the gases present in the chamber were CH_4/H_2/Ar with a ratio of 1.2/3/400. The deposition rate was approximately 0.05 nm/sec. The patterns were created using a JEOL 8100FS ebeam lithography system. An HSQ resist was spin-coated and exposed with EBL to form a mask for the consequent RIE etching that was done with RIE Oxford PlasmaLab 100, and the etching gases was Florine and Oxygen. Afterward, the resist was removed.

Transmission Measurements

An inverted microscope equipped with a spectrometer consisting of a 303 mm-focal-length monochromator and Andor Newton electron multiplication charge-coupled device (EM-CCD) camera was utilized for optical measurements. A linearly polarized broadband halogen light source was used. Transmitted light was collected from a 50 × 50 μm^2 area using a 5× Nikon microscope objective with a numerical aperture of 0.15. Clean regions of quartz were used as reference materials in all transmission measurements.

Photoluminescence Measurements

Measurement was carried out in a homemade photoluminescence setup. HeNe at a wavelength of 545 nm was used as the excitation source. The focused laser beam was coupled to an upright microscope (Nikon Eclipse Ti−U) with a computer-controlled x-y piezo stage (Thorlabs MLS203). Emitted and reflected beams from the sample are then filtered through a 550 nm long pass filter and coupled into a spectrometer (Andor Technology) containing a multiplication charge-coupled device (EM-CCD) (Andor Newton). Each map was constructed from an area of 150 × 150 μm^2 with an x-y step resolution of 2 μm.

FDTD Simulations

Electromagnetic wave numerical calculations were performed by using the finite-difference time-domain simulation software package Ansys Lumerical. A unit cell of the structure was simulated using periodic boundary conditions along the x and y axes and perfectly matched layers (PML) along the propagation of electromagnetic waves (z-axis). Plane waves were launched incident to the unit cell along the +z direction. A mesh override was set over the UNCD disks to 2 × 2 × 2 nm, and a mesh override of 1 × 1 × 1 nm in 1 nm thick MoS_2 was used. The refractive index for UNCD was taken from ellipsometry measurements and modeled using a Cauchy model with absorption tail, while the refractive index for quartz was set to a constant of 1.45 with an FDTD background index of 1. The refractive index of MoS_2 was taken from Yim et al.[44] The roughness of UNCD was modeled using a roughness function in the lumerical space by creating a random matrix of values in the k space defined by the x and y span.

ASSOCIATED CONTENT

Data Availability Statement

Data underlying the results presented in this paper are not publicly available at this time but may be obtained from the authors upon reasonable request.

Supporting Information

The Supporting Information is available free of charge at https://pubs.acs.org/doi/10.1021/acsaom.3c00071.

Effect of gap distance on simulated magnetic and electric anapoles, simulated and measured effect of gap distance on transmission effect of UNCD roughness on anapole modes, spectral photoluminescence (PDF)

https://doi.org/10.1021/acsaom.3c00071
ACS Appl. Opt. Mater. 2023, 1, 1627−1633

AUTHOR INFORMATION

Corresponding Author

Koray Aydin − *Department of Electrical and Computer Engineering, Northwestern University, Evanston, Illinois 60208, United States;* orcid.org/0000-0002-3268-2216; Email: aydin@northwestern.edu

Authors

Edgar Palacios − *Department of Electrical and Computer Engineering, Northwestern University, Evanston, Illinois 60208, United States*

Anirudha V. Sumant − *Center for Nanoscale Materials, Argonne National Laboratory, Lemont, Illinois 60439, United States;* orcid.org/0000-0002-6028-0038

Akshay A. Murthy − *Department of Materials Science and Engineering, Northwestern University, Evanston, Illinois 60208, United States*

Sina Abedini Dereshgi − *Department of Electrical and Computer Engineering, Northwestern University, Evanston, Illinois 60208, United States;* orcid.org/0000-0003-2929-0817

Vinayak P. Dravid − *Department of Materials Science and Engineering, Northwestern University, Evanston, Illinois 60208, United States; Northwestern University Atomic and Nanoscale Characterization Experimental (NUANCE) Center, Northwestern University, Evanston, Illinois 60208, United States;* orcid.org/0000-0002-6007-3063

Complete contact information is available at: https://pubs.acs.org/10.1021/acsaom.3c00071

Notes

The authors declare no competing financial interest.

ACKNOWLEDGMENTS

This work is supported by the Air Force Office of Scientific Research under award number FA9550-22-1-0300. This material is partially supported by the National Science Foundation under Grant No. DMR-1929356. This work made use of the EPIC, Keck-II, SPID facilities of Northwestern University's NUANCE Center, which has received support from the Soft and Hybrid Nanotechnology Experimental (SHyNE) Resource (NSF ECCS-1542205); the MRSEC program (NSF DMR-1720319) at the Materials Research Center; the International Institute for Nanotechnology (IIN); the Keck Foundation; and the State of Illinois, through the IIN. Also, use of the Center for Nanoscale Materials, an Office of Science user facility, was supported by the U.S. Department of Energy, Office of Science, Office of Basic Energy Sciences, under Contract No. DE-AC02-06CH11357. A.A.M. gratefully acknowledges support from the Ryan Fellowship and the IIN at Northwestern University.

REFERENCES

(1) Cubukcu, E.; Kort, E. A.; Crozier, K. B.; Capasso, F. Plasmonic laser antenna. *Appl. Phys. Lett.* **2006**, *89* (9), No. 093120.

(2) Oulton, R. F.; Sorger, V. J.; Zentgraf, T.; Ma, R. M.; Gladden, C.; Dai, L.; Bartal, G.; Zhang, X. Plasmon lasers at deep subwavelength scale. *Nature* **2009**, *461* (7264), 629−32.

(3) Zheludev, N. I.; Prosvirnin, S. L.; Papasimakis, N.; Fedotov, V. A. Lasing spaser. *Nat. Photonics* **2008**, *2* (6), 351−354.

(4) Esmaeili-Rad, M. R.; Salahuddin, S. High performance molybdenum disulfide amorphous silicon heterojunction photodetector. *Sci. Rep.* **2013**, *3* (1), 2345.

(5) Ross, J. S.; Rivera, P.; Schaibley, J.; Lee-Wong, E.; Yu, H.; Taniguchi, T.; Watanabe, K.; Yan, J.; Mandrus, D.; Cobden, D.; Yao, W.; Xu, X. Interlayer Exciton Optoelectronics in a 2D Heterostructure p-n Junction. *Nano Lett.* **2017**, *17* (2), 638−643.

(6) Xie, C.; Mak, C.; Tao, X.; Yan, F. Photodetectors Based on Two-Dimensional Layered Materials Beyond Graphene. *Adv. Funct. Mater.* **2017**, *27* (19), No. 1603886.

(7) Cao, L.; White, J. S.; Park, J. S.; Schuller, J. A.; Clemens, B. M.; Brongersma, M. L. Engineering light absorption in semiconductor nanowire devices. *Nat. Mater.* **2009**, *8* (8), 643−647.

(8) Hao, L. Z.; Gao, W.; Liu, Y. J.; Han, Z. D.; Xue, Q. Z.; Guo, W. Y.; Zhu, J.; Li, Y. R. High-performance n-MoS2/i-SiO2/p-Si heterojunction solar cells. *Nanoscale* **2015**, *7* (18), 8304−8308.

(9) Pradhan, S. K.; Xiao, B.; Pradhan, A. K. Enhanced photoresponse in p-Si/MoS2 heterojunction-based solar cells. *Sol. Energy Mater. Sol. Cells* **2016**, *144*, 117−127.

(10) Willets, K. A.; Van Duyne, R. P. Localized surface plasmon resonance spectroscopy and sensing. *Annu. Rev. Phys. Chem.* **2007**, *58* (1), 267−297.

(11) Khurgin, J. B. How to deal with the loss in plasmonics and metamaterials. *Nat. Nanotechnol.* **2015**, *10* (1), 2−6.

(12) Evans, C. I.; Zolotavin, P.; Alabastri, A.; Yang, J.; Nordlander, P.; Natelson, D. Quantifying Remote Heating from Propagating Surface Plasmon Polaritons. *Nano Lett.* **2017**, *17* (9), 5646−5652.

(13) Herzog, J. B.; Knight, M. W.; Natelson, D. Thermoplasmonics: quantifying plasmonic heating in single nanowires. *Nano Lett.* **2014**, *14* (2), 499−503.

(14) Zolotavin, P.; Alabastri, A.; Nordlander, P.; Natelson, D. Plasmonic Heating in Au Nanowires at Low Temperatures: The Role of Thermal Boundary Resistance. *ACS Nano* **2016**, *10* (7), 6972−6979.

(15) Kryder, M. H.; Gage, E. C.; McDaniel, T. W.; Challener, W. A.; Rottmayer, R. E.; Ju, G.; Hsia, Y.-T.; Erden, M. F. Heat Assisted Magnetic Recording. *Proc. IEEE* **2008**, *96* (11), 1810−1835.

(16) Wu, C.; Neuner, B., III; John, J.; Milder, A.; Zollars, B.; Savoy, S.; Shvets, G. Metamaterial-based integrated plasmonic absorber/emitter for solar thermo-photovoltaic systems. *J. Opt.* **2012**, *14* (2), 024005.

(17) Reddy, H.; Guler, U.; Kudyshev, Z.; Kildishev, A. V.; Shalaev, V. M.; Boltasseva, A. Temperature-Dependent Optical Properties of Plasmonic Titanium Nitride Thin Films. *ACS Photon.* **2017**, *4* (6), 1413−1420.

(18) Guler, U.; Shalaev, V. M.; Boltasseva, A. Nanoparticle plasmonics: going practical with transition metal nitrides. *Mater. Today* **2015**, *18* (4), 227−237.

(19) Li, W.; Guler, U.; Kinsey, N.; Naik, G. V.; Boltasseva, A.; Guan, J.; Shalaev, V. M.; Kildishev, A. V. Refractory plasmonics with titanium nitride: broadband metamaterial absorber. *Adv. Mater.* **2014**, *26* (47), 7959−7965.

(20) Razmjooei, N.; Ko, Y. H.; Simlan, F. A.; Magnusson, R. Resonant reflection by microsphere arrays with AR-quenched Mie scattering. *Opt. Express* **2021**, *29* (12), 19183−19192.

(21) Moitra, P.; Slovick, B. A.; Li, W.; Kravchencko, I. I.; Briggs, D. P.; Krishnamurthy, S.; Valentine, J. Large-Scale All-Dielectric Metamaterial Perfect Reflectors. *ACS Photon.* **2015**, *2* (6), 692−698.

(22) Slovick, B.; Yu, Z. G.; Berding, M.; Krishnamurthy, S. Perfect dielectric-metamaterial reflector. *Phys. Rev. B* **2013**, *88* (16), No. 165116.

(23) Aliofkhazraei, M. *Handbook of Nanoparticles*; Springer International Publishing, 2015.

(24) Yuan, S.; Qiu, X.; Cui, C.; Zhu, L.; Wang, Y.; Li, Y.; Song, J.; Huang, Q.; Xia, J. Strong Photoluminescence Enhancement in All-Dielectric Fano Metasurface with High Quality Factor. *ACS Nano* **2017**, *11* (11), 10704−10711.

(25) Zhang, X.; Choi, S.; Wang, D.; Naylor, C. H.; Johnson, A. T. C.; Cubukcu, E. Unidirectional Doubly Enhanced MoS2 Emission via Photonic Fano Resonances. *Nano Lett.* **2017**, *17* (11), 6715−6720.
(26) Wang, R.; Dal Negro, L. Engineering non-radiative anapole modes for broadband absorption enhancement of light. *Opt. Express* **2016**, *24* (17), 19048−19062.
(27) Miroshnichenko, A. E.; Evlyukhin, A. B.; Yu, Y. F.; Bakker, R. M.; Chipouline, A.; Kuznetsov, A. I.; Luk'yanchuk, B.; Chichkov, B. N.; Kivshar, Y. S. Nonradiating anapole modes in dielectric nanoparticles. *Nat. Commun.* **2015**, *6* (1), 8069.
(28) Totero Gongora, J. S.; Miroshnichenko, A. E.; Kivshar, Y. S.; Fratalocchi, A. Anapole nanolasers for mode-locking and ultrafast pulse generation. *Nat. Commun.* **2017**, *8* (1), 15535.
(29) Grinblat, G.; Li, Y.; Nielsen, M. P.; Oulton, R. F.; Maier, S. A. Efficient Third Harmonic Generation and Nonlinear Subwavelength Imaging at a Higher-Order Anapole Mode in a Single Germanium Nanodisk. *ACS Nano* **2017**, *11* (1), 953−960.
(30) Sabri, L.; Huang, Q.; Liu, J. N.; Cunningham, B. T. Design of anapole mode electromagnetic field enhancement structures for biosensing applications. *Opt. Express* **2019**, *27* (5), 7196−7212.
(31) Liu, S. D.; Fan, J. L.; Wang, W. J.; Chen, J. D.; Chen, Z. H. Resonance Coupling between Molecular Excitons and Nonradiating Anapole Modes in Silicon Nanodisk-J-Aggregate Heterostructures. *ACS Photon.* **2018**, *5* (4), 1628−1639.
(32) Talebi, N.; Guo, S.; van Aken, P. A. Theory and applications of toroidal moments in electrodynamics: their emergence, characteristics, and technological relevance. *Nanophotonics* **2018**, *7* (1), 93−110.
(33) Lynch, J.; Guarneri, L.; Jariwala, D.; van de Groep, J. Exciton resonances for atomically-thin optics. *J. Appl. Phys.* **2022**, *132* (9), No. 091102.
(34) Kumar, P.; Lynch, J.; Song, B.; Ling, H.; Barrera, F.; Kisslinger, K.; Zhang, H.; Anantharaman, S. B.; Digani, J.; Zhu, H.; Choudhury, T. H.; et al. Light−matter coupling in large-area van der Waals superlattices. *Nat. Nanotechnol.* **2022**, *17* (2), 182−189.
(35) Zhang, H.; Abhiraman, B.; Zhang, Q.; Miao, J.; Jo, K.; Roccasecca, S.; Knight, M. W.; Davoyan, A. R.; Jariwala, D. Hybrid exciton-plasmon-polaritons in van der Waals semiconductor gratings. *Nature Commun.* **2020**, *11* (1), No. 3552.
(36) Tóth, S.; Budai, J.; Veres, M.; Koós, M. Optical properties of nano- and ultrananocrystalline diamond thin layers in the UV and visible spectral range. *IOP Conf. Ser.: Mater. Sci. Eng.* **2018**, *426* (1), 012049.
(37) Aspnes, D. E.; Theeten, J. B.; Hottier, F. Investigation of effective-medium models of microscopic surface roughness by spectroscopic ellipsometry. *Phys. Rev. B* **1979**, *20* (8), 3292.
(38) Luk'yanchuk, B.; Paniagua-Domínguez, R.; Kuznetsov, A. I.; Miroshnichenko, A. E.; Kivshar, Y. S. Hybrid anapole modes of high-index dielectric nanoparticles. *Phys. Rev. A* **2017**, *95* (6), No. 063820.
(39) Zenin, V. A.; Evlyukhin, A. B.; Novikov, S. M.; Yang, Y.; Malureanu, R.; Lavrinenko, A. V.; Chichkov, B. N.; Bozhevolnyi, S. I. Direct amplitude-phase near-field observation of higher-order anapole states. *Nano Lett.* **2017**, *17* (11), 7152−7159.
(40) Murthy, A. A.; Stanev, T. K.; Dos Reis, R.; Hao, S.; Wolverton, C.; Stern, N. P.; Dravid, V. P. Direct visualization of electric-field-induced structural dynamics in monolayer transition metal dichalcogenides. *ACS Nano* **2020**, *14* (2), 1569−1576.
(41) Murthy, A. A.; Stanev, T. K.; Cain, J. D.; Hao, S.; LaMountain, T.; Kim, S.; Speiser, N.; Watanabe, K.; Taniguchi, T.; Wolverton, C.; Stern, N. P.; Dravid, V. P. Intrinsic transport in 2D heterostructures mediated through h-BN tunneling contacts. *Nano Lett.* **2018**, *18* (5), 2990−2998.
(42) Ciraci, C.; Vidal-Codina, F.; Yoo, D.; Peraire, J.; Oh, S.-H.; Smith, D. R. Impact of surface roughness in nanogap plasmonic systems. *ACS Photon.* **2020**, *7* (4), 908−913.
(43) Liu, Z.; Amani, M.; Najmaei, S.; Xu, Q.; Zou, X.; Zhou, W.; Yu, T.; Qiu, C.; Birdwell, A. G.; Crowne, F. J.; Vajtai, R.; et al. Strain and structure heterogeneity in MoS2 atomic layers grown by chemical vapour deposition. *Nat. Commun.* **2014**, *5* (1), 5246.
(44) Yim, C.; O'Brien, M.; McEvoy, N.; Winters, S.; Mirza, I.; Lunney, J. G.; Duesberg, G. S. Investigation of the optical properties of MoS2 thin films using spectroscopic ellipsometry. *Appl. Phys. Lett.* **2014**, *104* (10), 103114.

https://doi.org/10.1021/acsaom.3c00071
ACS Appl. Opt. Mater. 2023, 1, 1627−1633